The Iraqi Journal for Mechanical and Material Engineering, Vol.22, No3, June.2023

# EXPERIMENTAL AND NUMERICAL ANALYSIS OF NEW CURVED CONFIGURATION OF HEAT SINKS

**Hiba K. Mohsen[1]*** **Naseer Hamza[1]**
eng.mec.mas.20.2@qu.edu.iq naseer.hamza@qu.edu.iq
[1]Mechanical Engineering Department, College of Engineering, University of Al-Qadisiyah , Ad'Diwaniyah 58001, Iraq.

## ABSTRACT

In this study, the effect of changing geometry of the heat sinks on forced convection heat transfer and laminar fluid flow features in a rectangular channel has been studied experimentally and numerically of the circular fins and circular-cut fins heat sinks with straight continuous fins as reference comparison. For the experimental conditions, the Reynolds number value varied as 2418.56- 806.19 according to the variation of flow rate values. The wall heat flux was varied as 11.11, 31.11, 58.05, 83.05, 112.5, 155 kW/m$^2$. COMSOL Multiphysics was used to solve the governing equations under laminar flow conditions with air as the working fluid. To verify the accuracy of the analytical model, the simulation's optimal design was constructed and experimentally validated. The results indicated that circular-cut fins enhanced heat dissipation. Nusselt numbers for CCFs with Reynolds numbers of 797.7 and 2393.1 are roughly 83.6 and 132.4 at a heat flux of 11.1, kW/m2.

**Keywords: Heat sinks, Nusselt number, Laminar flow, Active Technique**

## INTRODUCTION

The thermal dissipation by electronic equipment components must be dispersed throughout the system in order to improve component reliability and system performance [1]. The use of an enhanced fin design, which effectively improves the performance of heat exchangers, is prevalent in a variety of applications in the electronic, air-conditioning, refrigeration, and processing industries. It is well known that the airflow in a compact heat exchanger is extremely complex due to the complex interactions between the airflow and the fin pattern. Convectional cooling of electronics, which typically employs forced-air cooling with a heat sink, has advantages in terms of cost, weight, structure, and dependability [2-9]. **Ibrahim et al. [10]** studied the theoretical and experimental effects of horizontal perforation on the thermal performance of longitudinal fins. The factors used for their analysis were geometrical, hydraulic, and thermal. By using a perforated fin, they obtained a temperature reduction of 8.5 °C. At low flow rates, their novel design was superior to the non-perforated in terms of heat dissipation. By increasing the size and

number of circular holes in the perforated fins, it was discovered that heat transfer was enhanced. **Choudhary et al. [5]** investigated experimentally the forced convective heat transfer and friction factor parameters of a circular pin-fin heat sink with and without stabilizers for inline and staggered configurations. The Reynolds number ranged between 6800 to 15100 in their investigation. The results indicated that pin fin heat sinks with wing (S/D) ratios of 2 and (Lw/D) ratios of 0.2 enhanced heat transmission more effectively. **Tariq et al. [11]** conducted numerical and experimental analyses of the advantages of many holes and slots in a plate-fin heat sink. It was determined that their innovative design of plate-fin heat sinks increases heat dissipation and reduces pressure drop. For a range of Re numbers from 13049 to 52195, the Nusselt number was 42.8% for perforations and 35.9% for plate-fin heat sinks with slots. **Maji et al. [12]** worked on numerical simulation utilising several perforated pin fin types (circular, diamond, and elliptical) for the augmentation of heat transfer rate versus pressure loss under forced convection. Results indicated that the Nusselt population increased by 12.1%, 13.9%, and 14.8% for circular, diamond-shaped, and elliptical perforation, respectively. In addition, the optimal size and number of perforations in a perforated fin produce the highest. **Fan et al. [13]** designed a unique cylindrical inclined fin heat sink that lowered overall thermal resistance by up to 59.1% with no pressure difference when compared to traditional straight fins. The enhanced thermal performance was a result of the disruption and initiation of the boundary layer at the leading edge of each fin. The use of streamline-shaped fins, such as elliptical, drop-shaped, and airfoil fins, to reduce flow resistance and maximise heat transfer across the flow channel is another strategy that has been experimentally and statistically investigated. **Moradikazerouni et al. [14]** analysed the cooling efficiency of a flat plate heat sink cooled by air under convective heat transfer. The length of the fins was 60 mm, the Reynolds number changed from $3.80 \times 10^3$ to $2.20 \times 10^4$, and the power supplied at the heat sink's base was 1000 W. They discovered that increasing the number and length of fins decreases the surface temperature of a plate by 25% and 20%, respectively. **Yu et al. [15]** examined experimentally and numerically a contemporary design of plate-pin fin heat sink (PPF). A simple plate fin heat sink was modified by inserting many column-shaped pins in a staggered pattern between the plate fins. Their findings suggested that under comparable conditions, PPF has 30% less thermal resistance than the conventional plate-fin heat sink tested. **Jeng and Tzeng [16]** investigated the performance of square fin arrays with variable streamwise and spanwise fin separations using the transient single-blow method. It was established that the fin Nusselt number of staggered square fins is roughly 20% greater than that of in-line circular fins, and that the best performing staggered square fins had inter-fin pitches of 1.5 in both the streamwise and spanwise directions. Similar tests were also conducted by **Akyol and Bilen [17]** and **Bilen et al. [18]**with hollow rectangular and tube fins, and matching relationships between fin arrangement and heat transfer performance were determined.

The main objective of this research is to discover the best heat sink geometry for maximising cooling performance. In this regard, experimental and numerical study was utilised to examine two novel fin geometries of a heat sinks, namely circular fins (CFs) and circular cut fins (CCFs) with traditional geometry straight continuous fins (SCFs) to compare best thermal performance under the same operating conditions.

## GOVERNING EQUATIONS

The equations of Navier-Stokes are used as governing equation for the forced convection fluid flow of the system. The following assumptions have been implemented:

1- The working fluid is air.

2- The flow is considered as steady, continuum, fully developed and three-dimensional.

3- The outside sides of the rectangular duct were insulated, with the exception of the heat sink base plate, for which a continuous heat flow emulating the electronic heater's heat production was required.

4- Material characteristics remained unchanged. Except for viscosity, fluid characteristics were temperature-independent.

5-Flow is considered laminar as Re is less than 2500.

6-Negligible radiation heat transfer.

7-The thermophysical properties of air are considered to be constant.

**For air flow**

Continuity equation:[19]

$$\frac{\partial u}{\partial x}+\frac{\partial v}{\partial y}+\frac{\partial w}{\partial z}=0 \quad (1)$$

x- momentum equation: [20]

$$\frac{\partial u}{\partial t}+u\frac{\partial u}{\partial x}+v\frac{\partial u}{\partial y}+w\frac{\partial u}{\partial z}=-\frac{1}{\rho_\infty}\frac{\partial p}{\partial x}+\nabla\cdot(\nu\nabla u) \quad (2)$$

y- momentum equation:

$$\frac{\partial v}{\partial t}+u\frac{\partial v}{\partial x}+v\frac{\partial v}{\partial y}+w\frac{\partial v}{\partial z}=-\frac{1}{\rho_\infty}\frac{\partial \hat{p}}{\partial y}+\nabla\cdot(\nu\nabla v) \quad (3)$$

z- momentum equation

$$\frac{\partial w}{\partial t}+u\frac{\partial w}{\partial x}+v\frac{\partial w}{\partial y}+w\frac{\partial w}{\partial z}=-\frac{1}{\rho_\infty}\frac{\partial p}{\partial z}+\nabla\cdot(\nu\nabla w) \quad (4)$$

Energy equation:

$$u\frac{\partial T}{\partial x}+v\frac{\partial T}{\partial y}+w\frac{\partial T}{\partial z}=\frac{K_f}{\rho_0 C_p}\left(\frac{\partial^2 T}{\partial x^2}+\frac{\partial^2 T}{\partial y^2}+\frac{\partial^2 T}{\partial z^2}\right) \quad (5)$$

**Dimensional governing equations in a heat sink**

$$K_s\left(\frac{\partial^2 T}{\partial x^2}+\frac{\partial^2 T}{\partial y^2}+\frac{\partial^2 T}{\partial z^2}\right)+\dot{q}_s=0 \quad (6)$$

**Domain and boundary conditions for computation:** [21]

*Inlet:*

$$T = T_{in} = 298\ K, v = u = w = 0$$

*Outlet:*

$$p = p_{\text{out}} = 0, u = w = 0, \frac{\partial T}{\partial y} = 0$$

*Adiabatic walls:*

$$u = v = w = 0, \frac{\partial T}{\partial z} = \frac{\partial T}{\partial x} = 0$$

*Heated wall:*

$$u = v = w = 0, q''_w = -k\frac{\partial T}{\partial x}$$

## NUMERICAL ANALYSIS

Using COMSOL Multiphysics version 5.6a CFD, the three-dimensional steady-state heat sink depicted in Figure 2 was simulated. Pre-Processing, Solver Execution, and Post-Processing are the three most important aspects in CFD estimations. During the pre-processing phase, the computational mesh is produced and the resolved objectives are determined. Configuration, boundary conditions, and numerical models are established in the second stage to activate the solver. Fluid flow parameters and exhibit geometry are utilised to identify the fins as aluminium. Solver continues till the commencement of the meeting. As soon as the solver finishes, the results are reviewed and the post is prepared. A computer with "11th Gen Intel(R) Core (TM) i7-1165G7 @ 2.80GHz" was used for the analysis. The force convection heat transfer was calculated using an open horizontal wind channel. The uniform air velocity at the entrance, air temperature of 26 degrees Celsius, no-slip boundary conditions, and ambient pressure at the outlet have all been implemented.

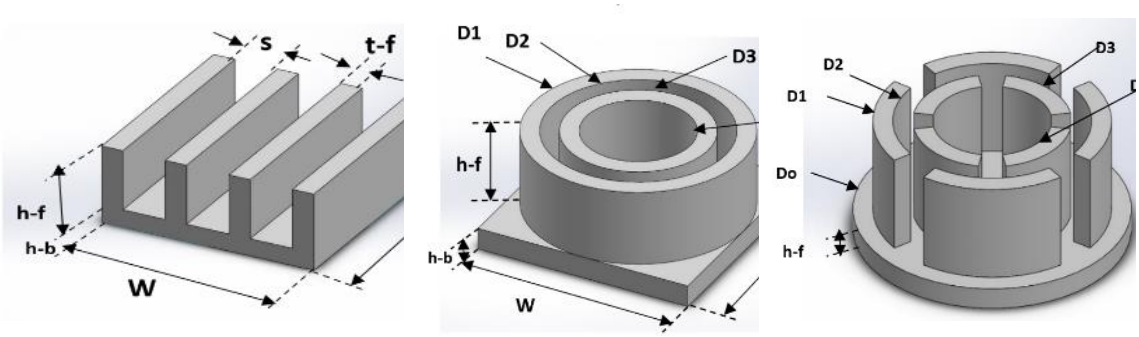


**a) SCFs** **b) CFs** **c) CCFs**

**Figure 2 Shows cases of study**

**Table 1 Dimensions of the cases study (mm)**

| Case study | W | L | h-b | h-f | s | t-f | t-p | d | Dh |
|---|---|---|---|---|---|---|---|---|---|
| **1.SCFs** | 60 | 60 | 6 | 20.6 | 12 | 6 | - | - | 15.17 |

| Case study | W | L | h-b | h-f | D1 | D2 | D3 | D4 | Dh |
|---|---|---|---|---|---|---|---|---|---|
| **2. CFs** | 60 | 60 | 6 | 21 | 60 | 50 | 40 | 30 | 10 |
| **3. CCFs** | - | - | 6 | 27 | 60 | 50 | 40 | 30 | 18 |

The numerical tests are performed on each type to ensure that solutions are independent of grid size based on comparisons of average Nusselt numbers as well as average temperature related to heat sinks. **Table 2** shown, the optimal mesh for SCFs in terms of accuracy and solution time is the normal grid of (451946). In **Figure. 3**.the mesh was bullied along channel and case study.

**Table 2 The average Nusselt number along SCFs using different mesh sizes.**

| Type of mesh | Number of nods | Average Nusselt number | Deviation in percentage |
|---|---|---|---|
| Extremely coarse | 23532 | 69.84 | |
| Extra Coarse | 42855 | 70.69 | 1.22% |
| Coarser | 82216 | 72.32 | 2.31% |
| Coarse | 198995 | 74.71 | 3.30% |
| Normal | 451946 | 75.56 | 1.14% |
| Fine | 1336101 | 75.64 | 0.11% |
| Finer | 3996683 | 75.81 | 0.22% |

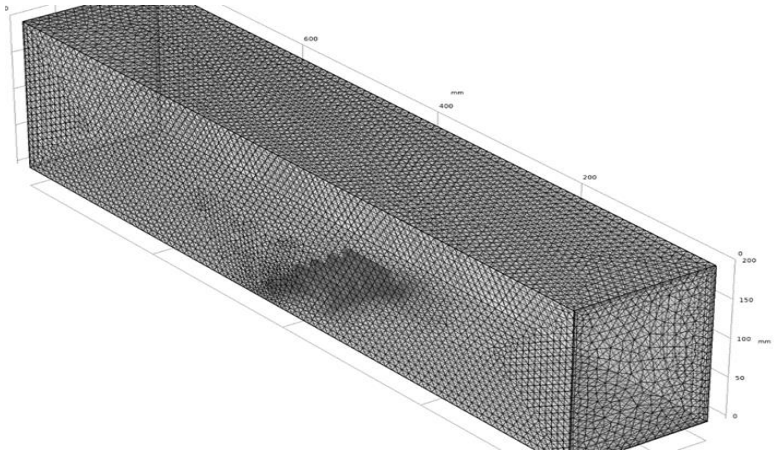


**Figure 3. 3D computational quadratic mesh of the domain**

## EXPERIMENTAL APPARATUS

**Figure 1** depicts a schema of the experimental apparatus and instruments used to study the thermal performance of a heat sink. As depicted in this diagram, the air was expelled by an electric blower. The wind tunnel was constructed from an acrylic plate measuring 2 mm in thickness. The rectangular flow channel measured 800 mm in length, 150 mm in width, and 200 mm in height. Inside the wind tunnel, the digital anemometer monitored the airflow velocity. To imitate actual working conditions, the base of the heat sink was put on the surface of the plate heater, which served as the heat source. The surface of the heater was coated with thermal silicone grease to reduce thermal contact resistance. The variable voltage transformer modified the plate heater's uniform heat output. The heater was embedded in a Bakelite rectangular rod with dimensions of 65 mm by 65 mm by 80 mm. Heat sinks were outfitted with twelve k-type thermocouples to measure airflow temperature at the heat sink entrance and exit. Two thermocouples were positioned 30 and 40 mm away from the heat sink. Similarly, two thermocouples were positioned 20 and 40mm after the heat sink. The data logger linked to the computer captured all of the thermocouple temperatures. A computerised manometer recorded the difference in pressure over the heat sink. To ensure precision and dependability, devices were calibrated and steady-state conditions were used to obtain experimental data. The heat sink was built using a CNC milling machine and an aluminium rod. The base of the heat sink measured 60 mm x 60 mm and 6 mm in height. The dimensions of the experimental examples are provided in Table 1.

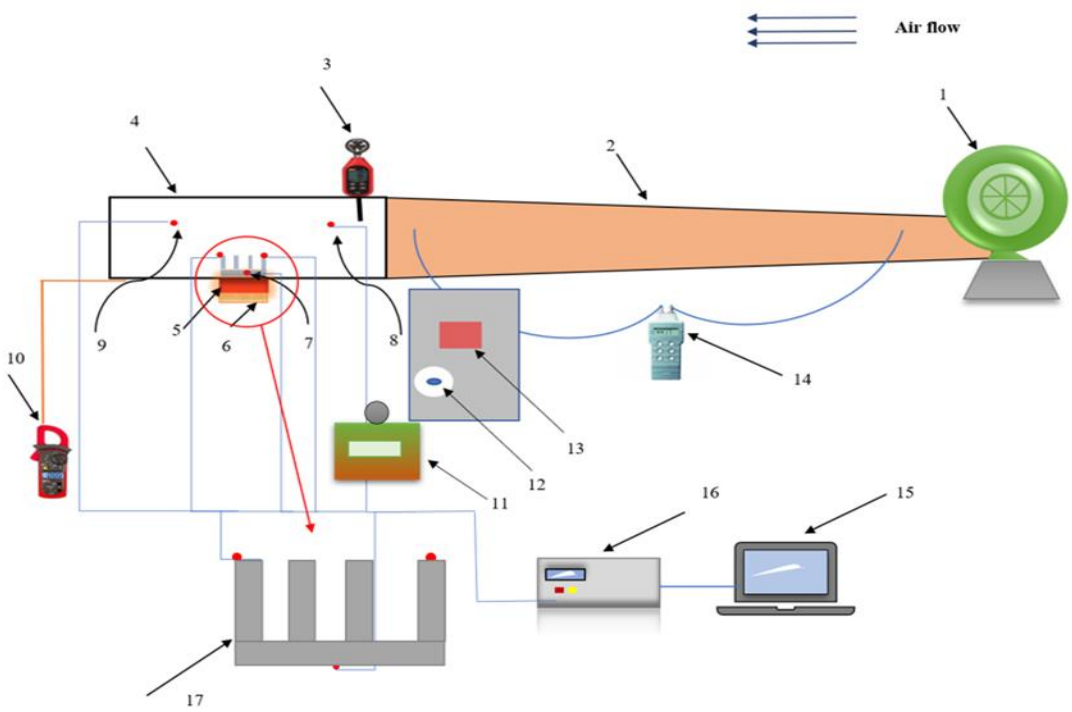


| | | | |
|---|---|---|---|
| 1 | Air blower | 10 | Clamp meter |
| 2 | Diffuser section | 11 | Variac |
| 3 | Digital anemometer | 12 | Air speed controller |
| 4 | Duct | 13 | Humidity meter |
| 5 | Plate heater | 14 | Pressure differential meter |
| 6 | Insulator | 15 | Notebook computer |
| 7 | Base thermocouples | 16 | Data logger |
| 8 | Inlet air thermocouple | 17 | Heat sink |
| 9 | Outlet air thermocouple | - | - |

**Figure 1 The Schematic diagram of experiment setup**

## DATA REDUCTION

In general, useful quantities such as the Nusselt number and thermal resistance can be calculated based on the temperature and velocity distribution. These calculations are extremely dependent on the wall's heat flux and average shear stress value**.[22]**

Average Nusselt number

$$N_u = \frac{h_{av} D_h}{k_a} \qquad (7)$$

Where: $$h_{av} = \frac{Q}{A_{surface}\left[T_S - \left(\frac{T_{out}+T_{in}}{2}\right)\right]} \quad (8)$$

Calculating the convective heat transfer rate from an electrically heated test surface using the relationship:

$$Q = m_a C_{pa}(T_{out} - T_{in}) \quad (9)$$

Reynolds number :

$$R_e = \frac{\rho_a V_{av} D_h}{\mu_a} \quad (10)$$

Where, the thermal Resistance can be calculated from:

$$R_{th} = \frac{T_s - T_{in}}{Q} \quad (11)$$

The maximum heat sinks temperature ($T_{surface}$) can be calculated from three reading of thermocouples measured heat sink temperatures as:

$$T_{surface} = \frac{T_1+T_2+T_3+T_4+T_5+T_6+T_7+T_8+T_{10}+T_{11}+T_{12}}{12} \quad (12)$$

**Experimental verification of a numerical simulation:**

Figure 4 depicts the comparison of numerical results with experimental results for all geometries in terms of temperature against height for the same heat flux, validating the functionality of the experimental device. Clearly, fin temperature decreases with increasing height. The difference between the experimental and numerical data can be attributed to two variables: the uncertainty of the measuring instruments and the assumptions underlying the numerical simulation. The largest differences between the experimental and numerical results are all less than 5%. This correlation demonstrates the accuracy of the numerical simulation and implies that the models can be used to forecast the performance of heat sinks' forms.

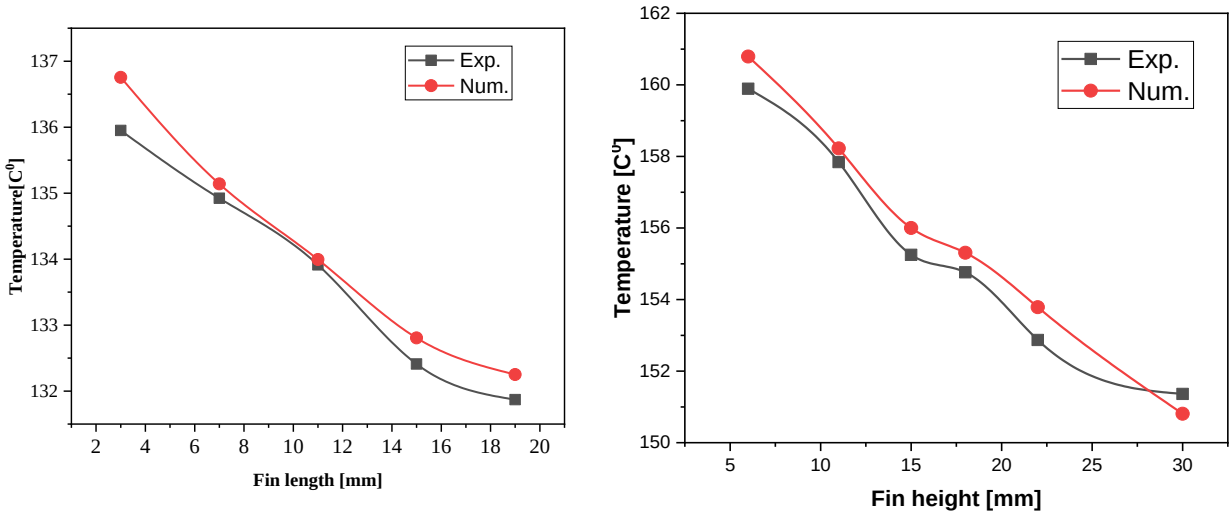


**(a) SCFs** **(b) CCFs**

**Figure 4. Comparison of the results of the temperature distribution along the z-axis of the fins between the real data of thermocouples and the numerical data.**

## RESULT AND DISCUSSION

### I. Numerical result

**Influence of the flow rate on the Nusselt number.**

Figure 5 present the variation of the Nusselt number with mass flow rate for the various configurations. The Nusselt number represents the proportion of heat transmission by convection to that by conduction. A rise in the Nusselt number suggests that the convective heat transmission has improved. In comparison to conventional heat sinks, the proposed heat sinks have a higher Nusselt number for both CFs and CCFs Fig 5 This increase in the Nusselt number is a result of the regrowth of the boundary layer as a result of continuous circulation. CFs and CCFs exhibit superior thermal enhancement compared to the other configurations. The reason beyond that is the positive effect of curvature of these configurations on the flow characteristics hydrodynamically and thermally. The curvature of circular path of proposed extended surfaces enhances the flow velocity which in its turn increases the Reynolds number and thus the Nusselt number and consequently increase the rate of heat dissipation, the matter which is examined later throughout this study. The design of the heat sinks has a significant impact on the Nusselt number. Consequently, the heat transfer enhancement rates of CFs and CCFs are greater than those of SCFs. At a flow rate of 0.00204 kg/s, the Nusselt numbers of CFs and CCFs are 137.65 and 142.32 respectively, and at flow rate, the Nusselt number of SCFs is 123.25.

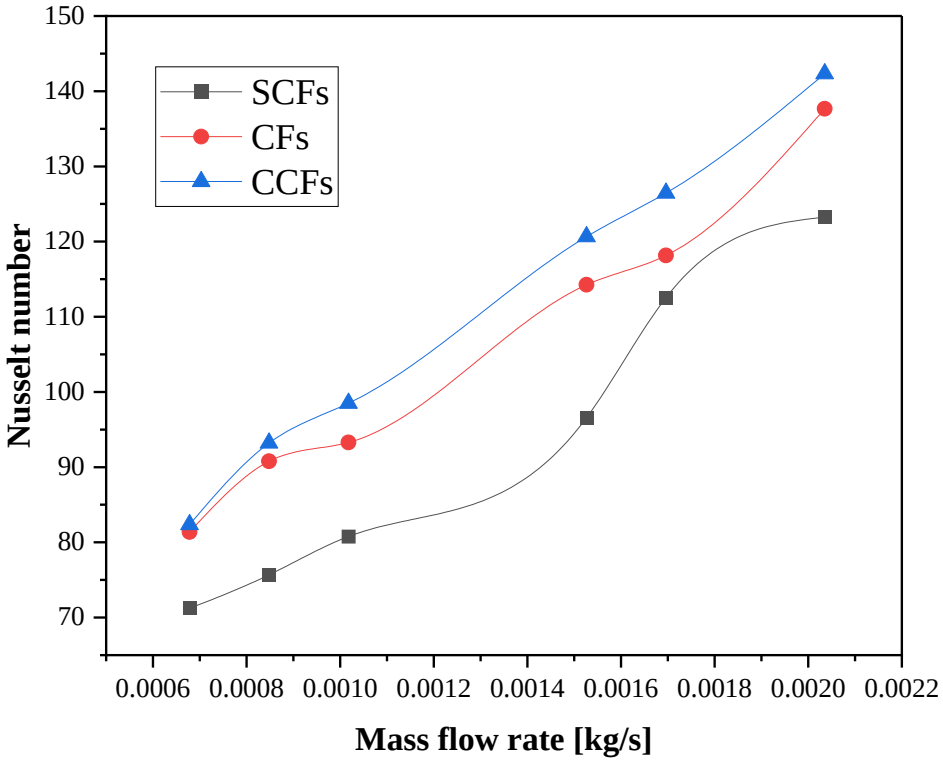


**Figure 5 Nusselt number versus mass flow rates for all configurations at q" = 31.1 kW/m2**

**Effect of the heat flux on the heat transfer coefficient**

The heat transfer coefficient is an important performance parameter when evaluating the thermal performance of the heat sinks. Figure 6 presents the variation of convection coefficient versus heat flux. For all configurations, the heat transfer coefficient increases exponentially with the increase of heat flux. As convective coefficient increases, the Nusselt number increases too. Thus, the optimal design is CCFs and CFs, due to an increasing in surface area and the curvature form that makes an increasing in heat dissipation.

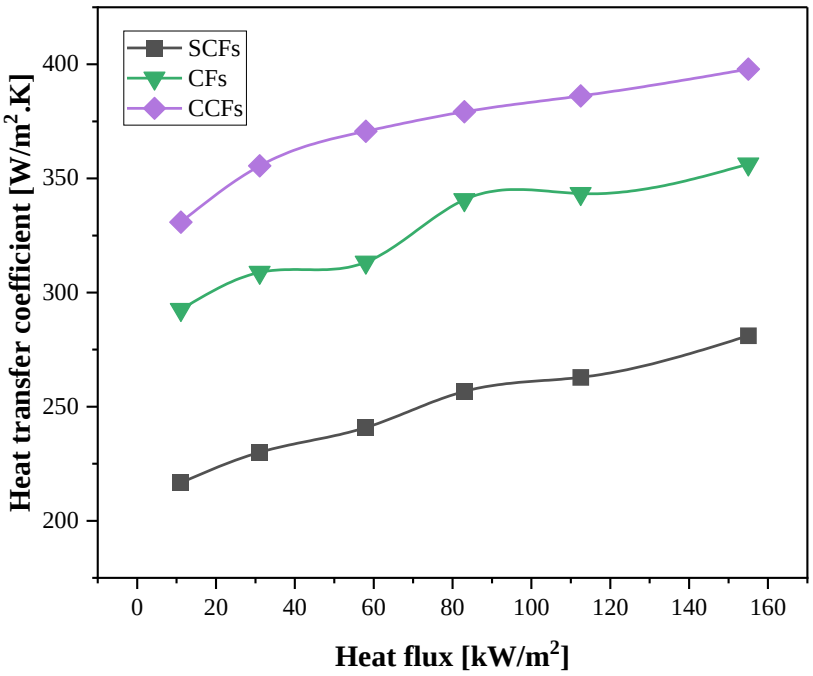


**Figure 6 Heat flux effect in different types of heat sink with heat transfer coefficient at (v=2.4 m/s).**

## Effect of air velocity on the thermal resistance at different configurations of a heat sinks

**Figure 7** illustrates the variations of thermal resistance at different velocities. For all geometries the thermal resistance decreases when velocity increases, this due to an increasing heat dissipation this in turn plays an important role in the thermal optimization process. From the figure the lowest thermal resistance was found at CCFs 0.66, and CFs was 0.77.

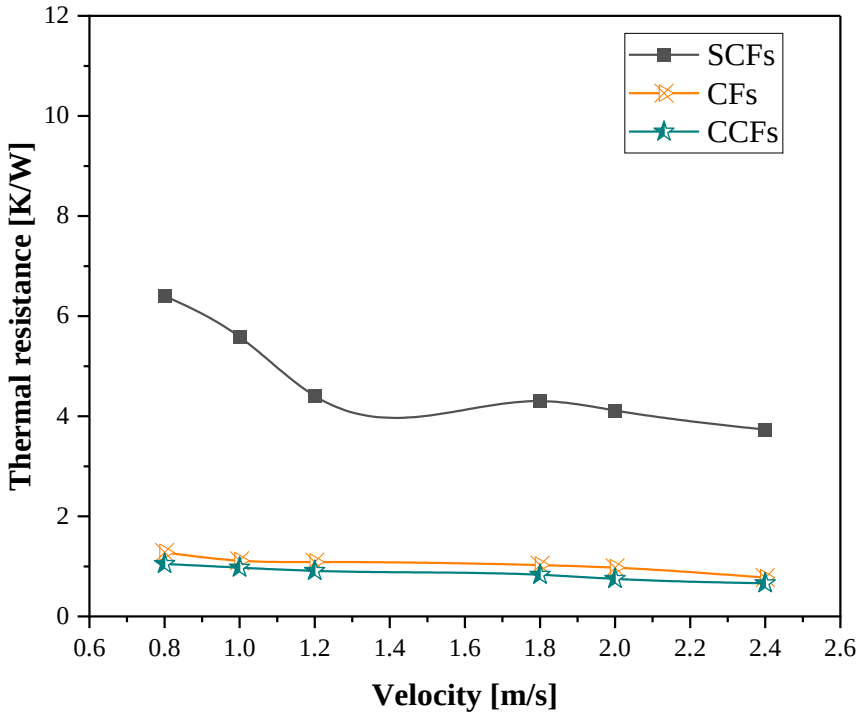


**Figure 7 Variation of thermal resistance with different air velocity at q" = 11.1kW/m$^2$**

**Figures 8** shows contour plots of the surface temperature distributions for all heat sink shapes examined at 1.8 m/s velocity, and power input (40W). The figure depicts the maximum temperature occurring at the heated bottom wall in relation to the heat sink because of the hight thermal conductivity of aluminium. The best heat dissipation was substantial between models (b) and (c). The circular fin and circular cut show a good performance in the process of heat dissipation. The reason beyond that is the positive effect of curvature of these configurations on the flow characteristics hydrodynamically and thermally. The curvature of circular path of proposed extended surfaces enhances the flow velocity which in its turn increases the Reynolds number and thus the Nusselt number and consequently increase the rate of heat dissipation, the matter which is examined later throughout this study. Furthermore, the rapid heat dissipation to the environment due to the increased surface area exposed to air, increasing airflow.

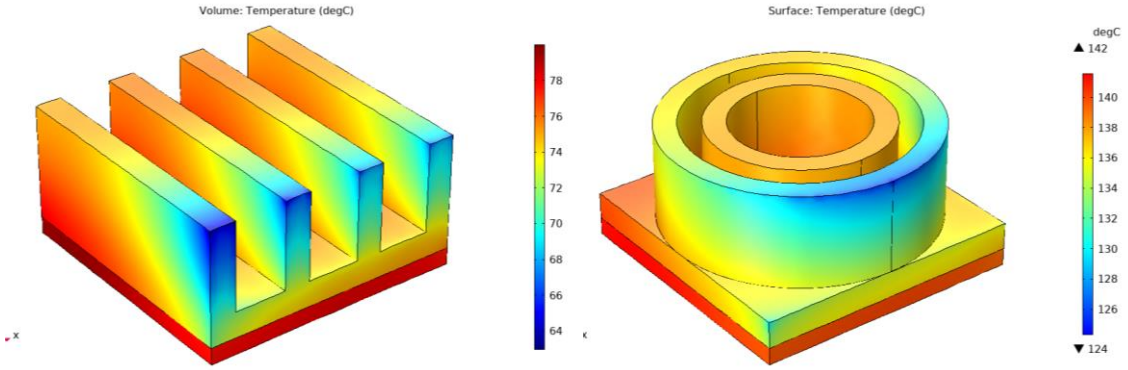


**a) SCFs** **b) CFs**

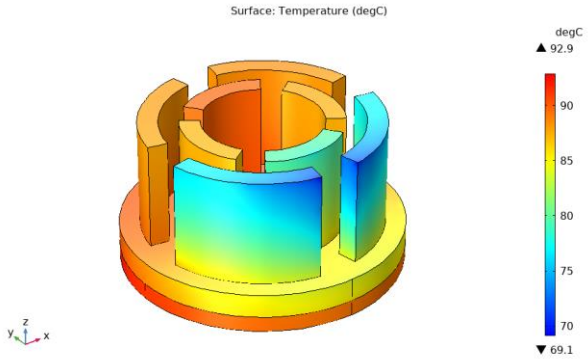


**c) CCFs**

**Figure 8 Temperature contour of the heat sinks in v= 1.8 m/s and p=40 W**

The pressure contour for all geometries showed in Figure 9. It was observed that the static pressure is slightly lower for heat sink due to the friction which is developed at surfaces of the fins.

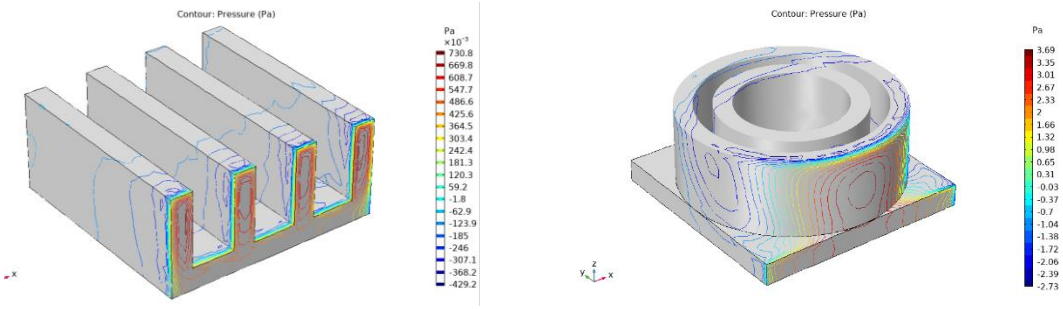


**a) SCFs** **b) CFs**

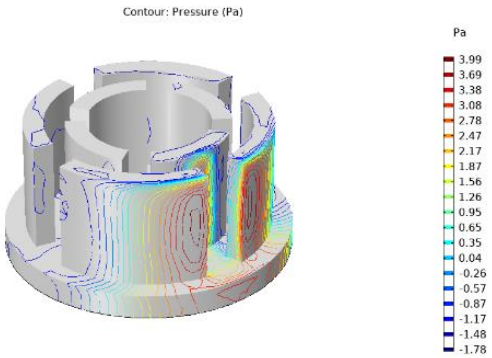


**c) CCFs**

**Figure 9 Pressure contour of the heat sinks in v= 1.8m/s and p=40 W.**

## II. Experimental results

### Effect of configurations on heat transfer coefficient at different Reynolds number.

**Figure 10** displays heat transfer as a function of fin geometry and Reynolds number for various fin sink types. In all cases, the graph illustrates that the heat transfer coefficient increases with rising Reynolds number. The most important reason for an increase in the heat transfer coefficient is that the amount of air and the flow potential of the removed heat will increase, resulting in an increase in the heat transfer coefficient. In addition, it is shown that the maximum heat transfer coefficient is reached in the circular-cut heat sink as a result of expanding the surface area of heat transfer through conduction/convection, which resulted in increased heat exchange with the air.

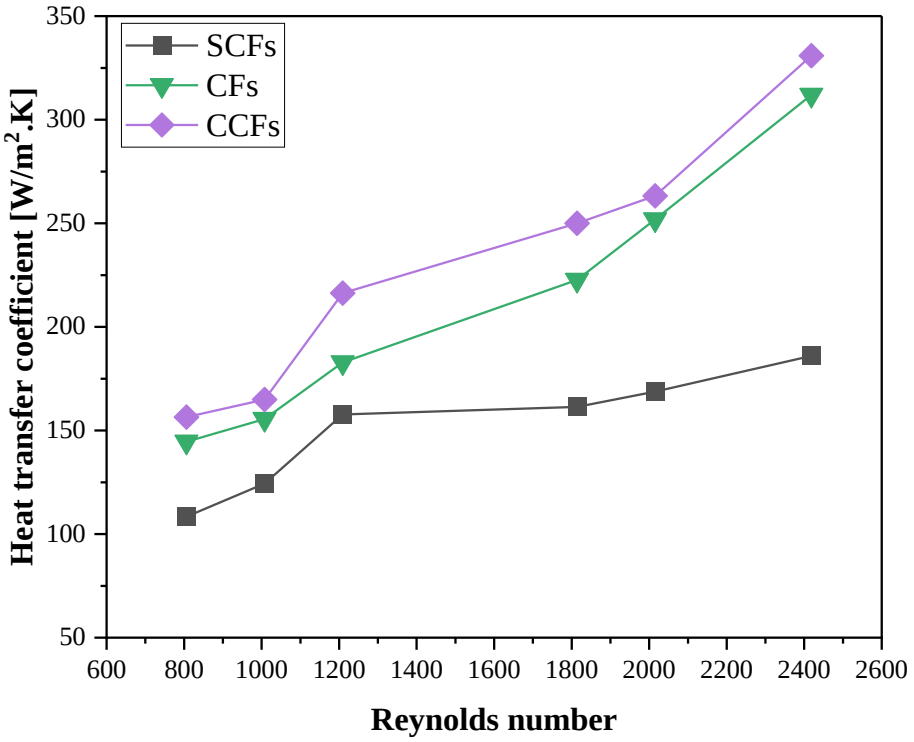


**Figure 10 Variation of heat transfer coefficient at different Reynolds number for q= 11.1kW/m$^2$**

**Figure 11** illustrates the connection between the Nusselt and Reynolds numbers. Nusselt number grew when Reynolds number increased for each heat sink. Clearly, the rise in Nusselt number is due to the increase in heat transfer coefficient resulting from the increase in air flow rate. At a heat flow of 11.1 kW/m2, the Nusselt numbers are approximately 83.6 and 132.4 for CCFs with Reynolds numbers of 797.7 and 2393.1, respectively.

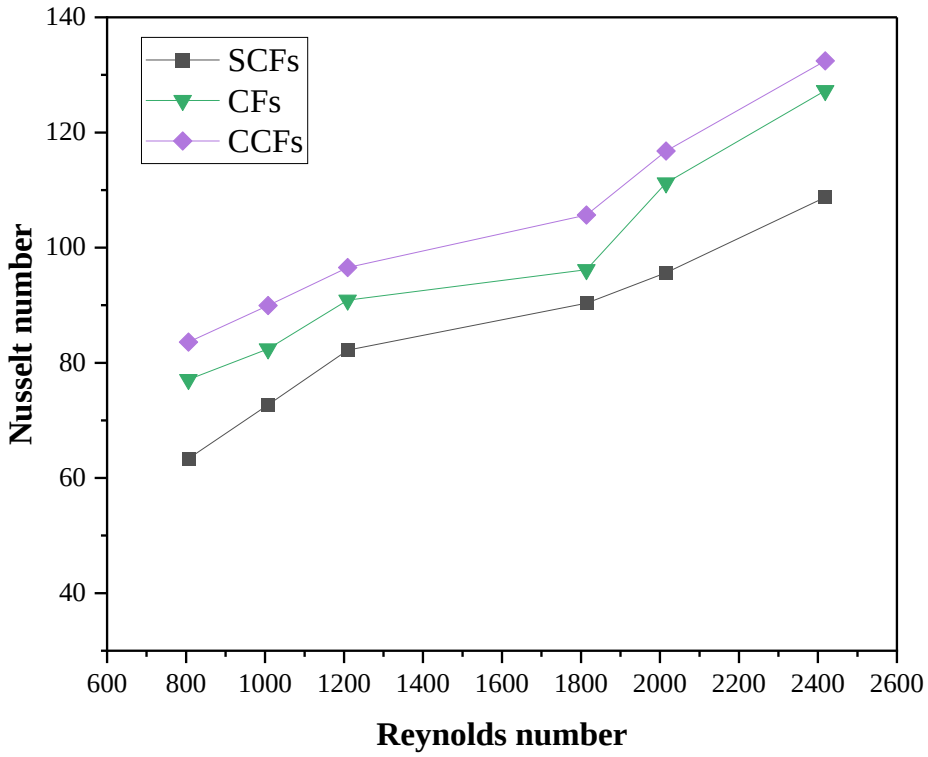


**Figure 11Nusselt number rate as a function of Reynolds number at (q1=11.1 kW/m2).**

## CONCLUSIONS

This study uses experimental and computational analysis to design a heat sink that is used in cooling of electronic devises. The effects of geometry on the laminar forced convection heat transfer in a three-dimensional rectangular duct with a constant heat flux boundary condition were numerically examined. This investigation found that the experimental result was good, identical to the numerical result. The emphasis was given on the heat transfer enhancement resulting from changing shape include SCFs, CFs, and CCFs, Reynolds number varying from 806.19 to 2418.56, and heat flux in the range of 11.1 kW/m2 to 155 kW/m2. The thermal performance for different values of heat flux are presented and discussed. The best configuration found in this study was the CCF because it had maximum dissipated heat. For a CCFs with Reynolds number of 797.7 and 2393.1, the values of Nusselt numbers about 83.6 and 132.4 at heat flux equal to 11.1 kW/m2.

## REFERENCES


1. Ahmed, H.E., *Optimization of thermal design of ribbed flat-plate fin heat sink.* Applied Thermal Engineering, 2016. **102**: p. 1422-1432.
2. Altun, A.H. and O. Ziylan, *Experimental investigation of the effects of horizontally oriented vertical sinusoidal wavy fins on heat transfer performance in case of natural convection.* International Journal of Heat and Mass Transfer, 2019. **139**: p. 425-431.
3. Awasarmol, U.V. and A.T. Pise, *An experimental investigation of natural convection heat transfer enhancement from perforated rectangular fins array at different inclinations.* Experimental Thermal and Fluid Science, 2015. **68**: p. 145-154.
4. Chingulpitak, S., et al., *Fluid flow and heat transfer characteristics of heat sinks with laterally perforated plate fins.* International Journal of Heat and Mass Transfer, 2019. **138**: p. 293-303.
5. Choudhary, V., M. Kumar, and A.K. Patil, *Experimental investigation of enhanced performance of pin fin heat sink with wings.* Applied Thermal Engineering, 2019. **155**: p. 546-562.
6. Duan, Z., et al., *Analysis of flow characteristics and pressure drop for an impinging plate fin heat sink with elliptic bottom profiles.* Applied Sciences, 2020. **10**(1): p. 225.
7. El Ghandouri, I., et al., *Thermal performance of a corrugated heat dissipation fin design: A natural convection numerical analysis.* International Journal of Heat and Mass Transfer, 2021. **180**: p. 121763.
8. Fan, Y., et al., *A simulation and experimental study of fluid flow and heat transfer on cylindrical oblique-finned heat sink.* International journal of heat and mass transfer, 2013. **61**: p. 62-72.
9. Huang, C.-H. and Y.-H. Chen, *An optimal design problem in determining non-uniform fin heights and widths for an impingement heat sink module.* Applied thermal engineering, 2014. **63**(2): p. 481-494.
10. Ibrahim, T.K., et al., *Experimental study on the effect of perforations shapes on vertical heated fins performance under forced convection heat transfer.* International Journal of Heat and Mass Transfer, 2018. **118**: p. 832-846.
11. Tariq, A., et al., *Comparative numerical and experimental analysis of thermal and hydraulic performance of improved plate fin heat sinks.* Applied Thermal Engineering, 2021. **182**: p. 115949.
12. Maji, A., D. Bhanja, and P.K. Patowari, *Numerical investigation on heat transfer enhancement of heat sink using perforated pin fins with inline and staggered arrangement.* Applied Thermal Engineering, 2017. **125**: p. 596-616.
13. Fan, Y., et al., *Process optimization with alternative carbon sources and modulation of secondary metabolism for enhanced ansamitocin P-3 production in Actinosynnema pretiosum.* Journal of Biotechnology, 2014. **192**: p. 1-10.

14. Moradikazerouni, A., et al., *Investigation of a computer CPU heat sink under laminar forced convection using a structural stability method.* International Journal of Heat and Mass Transfer, 2019. **134**: p. 1218-1226.
15. Yu, X., et al., *Development of a plate-pin fin heat sink and its performance comparisons with a plate fin heat sink.* Applied thermal engineering, 2005. **25**(2-3): p. 173-182.
16. Jeng, T.-M. and S.-C. Tzeng, *Pressure drop and heat transfer of square pin-fin arrays in in-line and staggered arrangements.* International Journal of Heat and Mass Transfer, 2007. **50**(11-12): p. 2364-2375.
17. Akyol, U. and K. Bilen, *Heat transfer and thermal performance analysis of a surface with hollow rectangular fins.* Applied Thermal Engineering, 2006. **26**(2-3): p. 209-216.
18. Bilen, K., U. Akyol, and S. Yapici, *Thermal performance analysis of a tube finned surface.* International Journal of Energy Research, 2002. **26**(4): p. 321-333.
19. Wang, X., et al., *Numerical investigation on hydraulic and thermal characteristics of micro latticed pin fin in the heat sink.* International Journal of Heat and Mass Transfer, 2020. **149**: p. 119157.
20. Liou, H.-J., S.-C. Wong, and Y.-C. Lin, *Revisit on the natural convection from horizontal multi-channel rectangular-fin heat sinks.* International Journal of Thermal Sciences, 2022. **171**: p. 107232.
21. Jaffal, H.M., H.S. Jebur, and A.A. Hussein, *Numerical and experimental investigations on the performance characteristics for different shapes pin fin heat sink.* IJOCAAS, 2018. **4**(3): p. 330-343.
22. Nilpueng, K., et al., *Effect of pin fin configuration on thermal performance of plate pin fin heat sinks.* Case Studies in Thermal Engineering, 2021. **27**: p. 101269.